1 Estimating the depth and evolution of intrusions at resurgent
2 calderas: Los Humeros (Mexico)

3 Stefano Urbani[1], Guido Giordano[1,2], Federico Lucci[1], Federico Rossetti[1], Valerio Acocella[1], Gerardo
4 Carrasco- Núñez[3]

5 [1]Dipartimento di Scienze, Università degli Studi Roma Tre, L.go S.L. Murialdo 1, I-00146 Rome, Italy
6 [2]CNR - IDPA c/o Università degli Studi di Milano, Via Luigi Mangiagalli, 34, 20133 Milano
7 [3]Centro de Geociencias, Universidad Nacional Autónoma de México, Campus UNAM Juriquilla, 76100, Queretaro,
8 Mexico

9 *Correspondence to*: Stefano Urbani (stefano.urbani@uniroma3.it)

10 **Abstract.** Resurgent calderas represent a target with high potential for geothermal exploration, as they are associated with

11 the shallow emplacement of magma, resulting in a widespread and long lasting hydrothermal activity. Therefore,

12 evaluating the thermal potential of resurgent calderas may provide important insights for geothermal exploitation.

13 Resurgence is classically attributed to the uplift of a block or dome resulting from the inflation of the collapse-forming

14 magma chamber due to the intrusion of new magma. The Los Humeros volcanic complex (LHVC; Mexico), consisting

15 of two nested calderas (the outer Los Humeros and the inner, resurgent, Los Potreros), represents an area of high interest

16 for geothermal exploration to optimize the current exploitation of the active geothermal field. Here we aim at better define

17 the characteristics of the resurgence in Los Potreros, by integrating field work with analogue models, evaluating the

18 spatio-temporal evolution of the deformation and the depth and extent of the intrusions responsible for the resurgence and

19 which may represent also the local heat source(s).

20 Structural field analysis and geological mapping show that Los Potreros area is characterized by several lava domes and

21 cryptodomes (with normal faulting at the top) that suggest multiple deformation sources localized in narrow areas.

22 The analogue experiments simulate the deformation pattern observed in the field, consisting of magma intrusions pushing

23 a domed area with apical graben. To define the possible depth of the intrusion responsible for the observed surface

24 deformations, we apply established relations to our experiments. These relations suggest that the magmatic source

25 responsible for the deformation is present at very shallow depths (hundreds of meters) which is in agreement with the

26 well data and field observations. We therefore propose that the recent deformation at LHVC is not a classical resurgence

27 associated with the bulk inflation of a deep magma reservoir; rather this is related to the ascent of shallow (<1 km) multiple

28 magma bodies. A similar multiple source model of the subsurface structure has been also proposed for other calderas with

29 an active geothermal system (Usu volcano, Japan) suggesting that the model proposed may have a wider applicability.

30 1 Introduction

31 Caldera resurgence consists of the uplift of part of the caldera floor. It is attributed to the emplacement of silicic magma

32 at different depth levels under limited viscosity contrasts with regard to the previously emplaced magma (Marsh, 1984;

33 Galetto et al., 2017). Resurgence is often associated with hydrothermal and ore forming processes, since the circulation

34 pattern and temperature gradients of geothermal fluids are structurally-controlled by the space-time distribution of faults

35 and fractures and by the depth and shape of the magmatic sources (e.g. Guillou Frottier et al., 2000; Prinbow et al., 2003;

36 Stix et al., 2003; Mueller et al., 2009). Therefore, the characterisation of the magma that drives resurgence (location, depth

37 and size) and of the factors controlling the release of the heat (permeability, fracture patterns, and fluid flow) have

38 important implications for the exploration and exploitation of renewable geothermal energy resources. In particular, the

39   estimation of the location, depth and geometry of the magmatic sources is crucial to define the possible geothermal and

40   mineral potential of resurgent calderas, allowing an economically sustainable exploration and exploitation of their resulted

41   natural resources.

42   On this regard, the intrusion of magma at different crustal depths has been proposed as the driving mechanism for

43   resurgence in many calderas worldwide (Linsday et al., 2001; Metrich et al., 2011; Kennedy et al., 2012, 2016; Lipman

44   et al., 2015; Brothelande et al., 2016). These natural cases may show different uplift styles (resurgent blocks or domes,

45   Acocella et al., 2001) and rates (from mm to cm per year), depending on the depth, volume and size of the magmatic

46   sources, but they share a common feature that is a coherent uplift of a significant part of the caldera floor.

47   This scenario is different from the occurrence of deformation patterns characterized by the widespread and delocalized

48   uplift of several minor portions of the caldera floor, as due to lava domes and/or cryptodomes, as for example observed

49   at Usu volcano (Japan, Matsumoto and Nakagawa, 2010; Tomya et al., 2010). A different depth and extent of the

50   responsible source(s) and, consequently, a different subsurface structure of the volcano is therefore suggested. A better

51   assessment of the subsurface structure in such cases has crucial implications for geothermal exploration, in order to

52   maximize the geothermal production.

53   In this regard, the Los Humeros Volcanic Complex (LHVC, Mexico) is an important geothermal target area, consisting

54   of two nested calderas with resurgence within the innermost one (Los Potreros caldera), commonly interpreted as due to

55   the uplift of a resurgence due to the inflation of a deep (several km) magma chamber (Fig. 1a, Norini et al., 2015).

56   The purpose of this work is to evaluate the depth to the intrusion(s) responsible for the uplift, also explaining the spatio-

57   temporal evolution of the observed deformation of the caldera floor. To achieve this goal, we integrate results from

58   structural field investigations carried out within the Los Potreros caldera with those derived from analogue experiments

59   specifically designed to constrain the depth of the deformation source(s) in volcanic caldera environments. Results

60   document discontinuous and small-scale (< 1 km) surface deformations generated from multiple and shallow (< 1 km)

61   magmatic bodies. These results should be taken into account for planning the future geothermal operations at the LHVC

62   and in other calderas showing similar surface deformation.

63   **2 Geological-structural setting**

64   LHVC is located at the eastern termination of the Trans Mexican Volcanic Belt (TMVB, see inset in Fig. 1a). The TMVB

65   is the largest Neogene volcanic arc in Mexico (~1000 km long and up to ~300 km wide), resulting from the Cenozoic

66   subduction of the Cocos and Rivera plates beneath the North American plate along the Middle American trench (Ferrari

67   et al., 2012, and references therein). The LHVC consists of two nested calderas formed during the Pleistocene: the outer

68   18 x 16 km Los Humeros caldera and the inner 10 x 8 km Los Potreros caldera (Fig.1a, Ferriz and Mahood, 1984; Norini

69   et al., 2015; Carrasco-Núñez et al., 2017b).

70   Based on updated stratigraphic and geochronological information, the evolution of the LHVC can be divided in three

71   main stages (Carrasco-Núñez et al., 2017b, 2018). The Pre-caldera volcanism extended between ca. 700 and 164 ka (based

72   on U-Th and ^{39}Ar/^{40}Ar datings: Carrasco-Núñez et al., 2018), showing evidence for an extended building phase leading

73   to the establishment of the large volume rhyolitic reservoir that fed the 115 km^3 caldera-forming, Xaltipan ignimbrite

74   eruption. The Caldera stage started at ca. 164 ka with the collapse of the Los Humeros caldera and ended with the eruption

75   of the 15 km^3 Zaragoza rhyodacite-andesite ignimbrite at 69 ka, associated with the collapse of the nested Los Potreros

76   caldera.

77   Carrasco-Núñez et al. (2018) interprets the Post Caldera stage (< 69 ka) as a Pleistocene resurgent phase, followed by the

78   Holocene activity characterized by intra-caldera basaltic to rhyolitic monogenetic volcanism. This hypothesis discards a

79   configuration of the magmatic plumbing system characterized by a unique, large and homogenized magma reservoir as

80   inferred for the Los Humeros activity during the Caldera Stage (e.g. Ferriz and Mohood, 1984; Verma, 1985) in favour of

81   a heterogeneous multi-layered system vertically distributed in the whole crust, with a deep (ca. 30 km) basaltic reservoir

82   feeding progressively shallower and smaller distinct stagnation layers, pockets and batches up to very shallow conditions

83   (1kbar, ca. 3km) (Lucci et al., under review).

84   In particular, during the early resurgent phase of the Post-Caldera stage, rhyolitic domes were emplaced along the northern

85   rim of the Los Humeros caldera, followed by the emplacement of less evolved lavas of trachyandesitic-trachytic

86   composition (Carrasco-Núñez et al., 2017b). The Holocene ring-fracture and bimodal magmatism is characterized by both

87   explosive and effusive activity, producing several lava flows and domes, as well as periods of dominant explosive activity

88   (e.g. the ca. 7 ka Cuicuiltic Member, Dávila-Harris and Carrasco-Núñez, 2014) from multiple vents located mostly along

89   both the inner and outer caldera ring faults. During this phase, less evolved lavas were erupted (from trachyandesite to

90   basalt) within and outside Los Humeros caldera, one of them corresponds to an olivine-bearing basaltic lava associated

91   with the formation of the Xalapasco crater (Fig. 1a). Trachytic lava flows are the most recent activity recorded by LHVC

92   at ca. 2.8 ky (Carrasco-Núñez et al., 2017b).

93   The reconstruction of the shallow stratigraphy in Los Potreros is chiefly derived from the information derived from the

94   available well logs (Figs. 1b-c Carrasco-Núñez et al., 2017a, b). Overall, the post-caldera units are lithologically

95   dominated by lava flows resting onto the ignimbrite deposits emplaced during caldera stage. Ignimbrites of the caldera

96   stage rest in turn on a thick sequence dominated by old andesite lavas dated at ca. 1.4-2.8 Ma (Carrasco-Núñez et al.,

97   2017a). The subsurface geometry of the pre- and syn-caldera products is better elucidated in Fig. 1b and 1c, which show

98   the in-depth geometry of the different magmatic products that are cross-correlated and projected along the N-S and E-W

99   direction, respectively. The N-S projection shows a constant depth of the top surface of the pre-caldera andesites that is

100 associated with a highly variable depth (up to 400 m) of the top surface of the syn-caldera Xaltipan ignimbrite. The W-E

101 projection shows a high depth variability of both the top surface of the pre-caldera group (up to 500 m between H-19 and

102 H-25 wells) and that of the Xaltipan ignimbrite (up to 400 m between H-19 and H-10 wells). Within this framework, a

103 remarkable feature is the presence of both basaltic and rhyolitic-dacitic lavas located at various depths (Carrasco-Núñez

104 et al., 2017a). In particular, the rhyolties-dacites are located mostly at the base (H-20 and H-26 wells) or within (H-05

105 well) the caldera group or within the old andesite sequence (H-25 and H-19 wells). On the other hand, the basalts are

106 located at various depths only within the pre-caldera andesite sequence, both at its base (in contact with the limestone

107 basement; H-5 and H-8 wells) and at its top (in contact with the base of the caldera sequence; H-10 well). Such bimodal

108 lava products, showing an irregular lateral distribution, are interpreted as subaerial volcanic episodes (Carrasco-Núñez et

109 al., 2017a).

110 The structure of the LHVC is controlled by a network of active extensional fault systems, consisting of NNW-SSE, N-S,

111 NE-SW and E-W fault strands cutting across the Los Potreros caldera floor. In particular, the following main faults were

112 recognised (Norini et al., 2015; Calcagno et al., 2018) (Fig.1a): (i) Maztaloya (NNW-SSE striking), (ii) Los Humeros and

113 Loma Blanca (N-S striking), (iii) Arroyo Grande (NE-SW striking), (iv) Las Viboras and Las Papas (E-W striking). Such

114 active fault system is interpreted as due to the recent/active resurgence of the Los Potreros Caldera, since the faults do not

115 show continuity beyond the caldera border, their scarps decrease in height towards the periphery of the caldera and the

116 dip-slip displacement vectors show a semi-radial pattern (Norini et al., 2015).

117 The source of the areal uplift is inferred to be the inflation of a saucer or cup shaped deep magmatic source elongated

118 NNW-SSE, upwarping a 8 x 4 km resurgent block, centred in the SE portion of the caldera, delimited to the W by the

119 NNW–SSE main faults, and toward the north, east and south by the caldera rim (Fig.1a, Norini et al., 2015).

120 The seismic activity in the period 1994-2017 is clustered along the Loma Blanca, Los Humeros and Arroyo Grande faults

121 (Lermo et al., 2018; Fig. 1a). Most of the earthquakes show a magnitude (Mw) between 1 and 2.5, and have been mainly

122 interpreted as induced by the geothermal exploitation activity (injection of fluids and hydrofracturing; Lermo et al., 2018).

123 Moreover, four major earthquakes (Mw= 3.2, 3.6, 3.9 and 4.2, at a depth of 1, 4, 2.2 and 1.8 km, respectively) have been

124 also reported, with focal depths close to the trace of the active faults (Loma Blanca and Los Humeros, Fig.1a). Such major

125 earthquakes have been interpreted as triggered by fault reactivation due to fluid/brine circulation injected from geothermal

126 wells (Lermo et al., 2018).

127 **3 Methods**

128 The scientific rationale adopted in this study is based on structural field work, combined with analogue models aimed to

129 constrain the depth of the deformation sources in the caldera domain.

130 **3.1 Structural field work**

131 Structural field work was carried out to evaluate the surface deformation related to the recent activity of the Los Potreros

132 caldera, in order to constrain the morphotectonic fingerprints of the resurgence. The geometry and distribution of the

133 observable faults and joints were defined at the outcrop scale by measuring their attitudes (strike and dip with the right-

134 hand rule) and spacing. Fault kinematics was assessed through classical criteria on slickensides fault surfaces, such as

135 Riedel shears and sheltering trails (Doblas, 1998). The geological-structural mapping of the studied area aims at

136 reconstructing the relationships between the post-caldera volcanic products and the structural features at the surface to

137 constrain the source and extent of the resurgence. To this purpose, interpretation of published geological map (Carrasco-

138 Núñez et al., 2017b) and geothermal well data has been also used.

139 **3.2 Analogue models: experimental set-up and scaling**

140 We performed three experiments simulating the ascent of a viscous intrusion in a brittle overburden with the aim to test

141 existing relationships between the depth of intrusion and the observed surface deformation. The experimental set-up (Fig.

142 2) consists of a 31 × 31 cm glass box filled with a sand pack (crust analogue) of variable thickness (T, of 30 and 50 mm,

143 respectively). In each experiment we imposed a layering using a non-cohesive marine sand below a layer of crushed silica

144 sand (grain size = 40-200 μm, cohesion = 300 Pa), fixing the thickness ratio of the two layers (T_u/T_l) to 1, to simulate the

145 stratigraphy in Los Potreros (stiffer post caldera lava flows above softer and less cohesive ignimbrite deposits emplaced

146 during the caldera collapse stage). At the base of the sand pack, a piston, controlled by an engine, pushes upward the

147 silicone (magma analogue) placed inside a cylinder 8 cm in diameter. The injection rate is fixed for all the experiments

148 to 2 mm/hr and each experiment was stopped at the onset of the silicone extrusion. Both sand and silicone physical

149 properties are listed in Table 1.

150 At the end of each experiment, the surface has been covered with sand to preserve their final topography and were wet

151 with water for cutting in sections to appreciate the subsurface deformation. Such sections were used to measure the mean

152 dip of the graben faults (θ) induced by the rising silicone. A digital camera monitored the top view deformation of each

153 experiment at 0.02 fps and a laser scanner, placed next to the camera, provided high-resolution data (maximum error ±

154 0.5 mm) of the vertical displacement that was used to measure in detail the geometrical features of the deformation i.e.

155 dome diameter (L_d), graben width (L_g) and dome flank mean dip (α). According to the Buckingham-Π theorem (Merle

156 and Borgia 1996 and references therein), our models need 7 independent dimensionless numbers to be properly scaled

157 (i.e. 10 variables minus three dimensions, table 1). Such dimensionless numbers can be defined as the ratios (Π) listed in

158   Table 2. Even if the values of Π_5 differ of two orders of magnitude in nature and in the experiments (1.8×10^{-8} and $6 \times$

159   10^{-10}, respectively), they are both largely <1, indicating that the ratio is a negligible value in both cases.

160   **4 Results**

161   **4.1 Local geology and structural data**

162   The outcropping post-caldera lithologies within the Los Potreros Caldera consist of: (1) the Cuicuiltic Member, which

163   blankets most of the surface of the upper half of the studied area; (2) basaltic lava flows filling the Xalapasco crater and

164   the NW portion of the caldera; and (3) trachyandesitic and trachytic lava domes and thick flows extending in the southern

165   half of the caldera and rhyolitic domes in its central part (Fig. 3). The more evolved lavas form four elliptical domes,

166   aligned N-S (Figs. 3, 4a): (i) a 2 long × 1.2 km wide trachytic dome located to the west of the Maztaloya and Los Humeros

167   faults, (ii) a 1 × 0.7 km trachyandesitic dome located at the northern tip of the Maztaloya fault, and (iii) two smaller (0.4

168   × 0.2 km) rhyolitic domes at the southern tip of the Los Humeros fault (LH-11 in Fig.3).

169   We identified three uplifted areas corresponding to the surface expression of the Loma Blanca, Arroyo Grande and Los

170   Humeros faults (labelled 1-2, 9 and 10 respectively in Fig. 3). The observed structures in these uplifted areas (joints and

171   faults) affect the deposits of the post-caldera phase. Based on field evidence, we also propose a revised interpretation of

172   the surface structures identified by previous studies (Norini et al., 2015) distinguishing between lineaments

173   (morphological linear scarps which are not associated with significant deformation and alteration at the outcrop scale),

174   active and inactive faults, associated with active and fossil alteration respectively (Fig. 3).

175   We present below a description of the structures mapped in the studied area, highlighting their temporal and spatial

176   relationships with the post-caldera geological formations. We identified two inactive faults (Maztaloya and Arroyo

177   Grande), a morphological lineament (Las Papas) and two currently active faults (Los Humeros and Loma Blanca). The

178   data number at each location is hereafter indicated with "n".

179   **4.1.1 Las Papas lineament (LH-07, LH-08)**

180   The E-W trending Las Papas scarp (Fig. 4b) is localised within the Cuicuiltic Member. Such lithologies do not show any

181   alteration or significant deformation (LH-07; Fig. 4c). We identified an erosional surface along the scarp, where unaltered

182   and undeformed Cuicuiltic rocks rest above a layered pyroclastic deposit (LH-08, Fig. 4d). The E-W trending

183   morphological lineaments defined by the Las Papas scarp is probably due to differential erosion of the softer layers of the

184   pyroclastic deposits, successively blanketed by the Cuicuiltic Member.

185   **4.1.2 Arroyo Grande (LH-09) and Maztaloya**

186   The NE-SW Arroyo Grande scarp (Fig.5a) exposed strongly altered and faulted (NW striking faults, mean attitude

187   N144°/68°, n = 8) lavas and ignimbrites unconformably covered by the unaltered Cuicuiltic Member (Fig.5b). The throw

188   observed at the outcrop-scale for the single fault strands is in the order of 0.5 m, with a dominant normal dip-slip

189   kinematics (slickenline pitch angle ranging from 99° to 106°). The inferred cumulative displacement at Arroyo Grande ~

190   is 10 m. Similarly, an outcrop on the Maztaloya scarp (in front of well H-6) shows altered trachyandesites covered by

191   unaltered Cuicuiltic rocks (Fig. 5c).

192   **4.1.3 Los Humeros (LH-10)**

193 The fault scarp of the N-S striking (mean attitude N174°/73°, n= 8) Los Humeros Fault is defined by the altered portions

194 of the Cuicuiltic Member. Fault population analysis reveals a dominant normal dip-slip (mean pitch angle 84°, n= 8)

195 kinematics, as documented by both Riedel shears and carbonate-quartz growth steps. The main fault plane is sutured by

196 a trachyandesitic extrusion (Fig. 5d), localised along an aligned N-S dome (LH-11 in Fig. 3). Moreover, ~150 m southward

197 from the outcrop of the fault scarp, a 5 × 3 m trachyandesitic plug shows vertical striation on its surface due to a subsurface

198 vertical flow of the trachyandesite (Fig. 5e). The observed displacement at the outcrop scale, as indicated by the height

199 of the fault scarp, is ~ 10 m.

200 **4.1.4 Loma Blanca (LH-01, LH-02)**

201 The Loma Blanca Fault system (LH-01 and LH-02) is located in correspondence of an active degassing area, where faults

202 and fractures are frequent.

203 The fault system localises on top of an elongated crest (within a graben) of a morphological bulge, ~ 1 km in diameter

204 and 30 m in height. At this location, the Cuicuiltic Member and the underlying trachyandesite lavas are strongly altered.

205 Evidence of stockwork veining and diffuse fracturing of the lavas suggests hydrofracturing and structurally controlled

206 fluid flow and alteration. A set of NNE-SSW striking conjugate extensional faulting and jointing (joint spacing ~1 m;

207 Fig. 5f) is observed. The faults (mean attitude N26°/71°) show a normal dip-slip kinematics (pitch ranging from 82° to

208 104°). Joint systems found in the Cuicuiltic Member strike sub-parallel to the faults (mean attitude N37°/72°, n= 14). The

209 inferred cumulative displacement of the faults, estimated by the depth of the apical graben, is ~ 5 m.

210 Summing up, the 22 mapped faults in all the structural outcrops of the area show a main NNW-SSE strike (Fig. 5g) with

211 a dominant dip slip movement (mean pitch angle of slickenlines 88°) which is sub-parallel to the N-S elongation of the

212 lava domes and the Xalapasco crater.

213 **4.2 Experimental results**

214 Here we show two representative experiments with increasing overburden thickness (experiments 5 and 6 with T= 30 and

215 50 mm respectively). Table 3 shows the measured parameters in the experiments.

216 Overall, the experiments show a similar deformation pattern: a first stage characterized by the uplift of a sub-circular

217 dome, bordered by inward dipping reverse faults, and a second stage characterized by the subsidence of the apical part of

218 the dome where normal faulting occurs (graben formation Fig. 6a-f). The reverse and normal faults are ring faults and are

219 associated with the formation of radial fractures from the dome centre.

220 Despite the T/D ratio, all the experiments show that both the dome diameter and graben width increase linearly with the

221 overburden thickness (ranging from 105 to 164 mm and from 14 to 58 mm respectively, Table 3, fig.7).

222 The dome diameter increases abruptly with time, becoming almost constant at an early stage of the experiment (fig.8a);

223 the graben width shows a similar pattern even if it enlarges slightly with time (after the first abrupt increase) as the silicone

224 rises towards the surface (fig.8b), suggesting that the intrusion depth has an higher influence on the graben width, in

225 agreement with (Brothelande and Merle, 2015).

226 **5 Discussion**

227   The distribution of the alteration patterns and deformation characteristics of the post caldera deposits can be used to infer

228   the origin and extent of the uplift within the LHVC. In particular, the involvement or not of the 7.4 ka Cuicuiltic Member

229   in the deformation and alteration allow constraining the spatio-temporal evolution of the surficial deformation and

230   associated uplifts in Los Potreros. Indeed, unaltered and undeformed deposits of the Cuicuiltic Member crops out along

231   the E-W Las Papas lineament and unconformably covers altered and faulted lavas and ignimbrites along the Arroyo

232   Grande and Maztaloya scarps. Alteration and deformation of the Cuicuiltic Member occurs along the Los Humeros Fault

233   scarp and within the apical graben of the Loma Blanca bulge. Moreover, the vertical striations of the trachyandesitic plug

234   near the Los Humeros fault scarp suggest that the ascent of the plug induced the uplift, the normal dip-slip faulting and

235   alteration of the Cuicuiltic.

236   All these observations suggest that Los Potreros is not a classic resurgent caldera (i.e. a caldera characterised by a large-

237   scale process localized in a single area) but is rather characterised by a discontinuous uplifting process in space and time,

238   inducing small-scale deformations at each pulse (Fig. 9a-d). In particular, it was active in the south and north-eastern

239   sector of the caldera, at Maztaloya and Arroyo Grande (Fig. 9a), prior to the deposition of the Cuicuiltic Member (~ 7.4

240   ka), and then moved towards N along the Los Humeros and Loma Blanca scarps during and post the eruption of the

241   Cuicuiltic (fig. 9b-d). Concerning the source of the deformation, the felsic lava found at the Los Humeros Fault scarp

242   shows a similar mineral assemblage of the felsic domes located further south (fig. 3); thus, the Los Humeros scarp may

243   represent the final stage (i.e. effusive eruption of felsic magmas, (Fig. 9c) of the uplift process, which is thus driven by

244   the ascent of relatively narrow (hundreds of meters) and highly viscous felsic magma batches. This is also supported by

245   the N-S elongation of the identified lava domes and Xalapasco crater which is sub-parallel to the orientation of the

246   measured fault planes (NNW-SSE) indicating that the observed deformation is closely related to the post-caldera

247   volcanism. The ascent of such magma bodies is inferred here to drive the recent uplift and deformation of the Loma

248   Blanca bulge, as suggested by the active fumaroles and extensive alteration of both the Cuicuiltic pyroclastics and post-

249   caldera lavas (Fig. 9d). The presence of such shallow magma bodies is also suggested by the four major earthquakes

250   recorded in Los Potreros, which have been previously interpreted to be induced by geothermal exploitation (Lermo et al.,

251   2018). However, since the magnitude of the seismic events induced by geothermal exploitation activities is usually lower

252   (i.e. < 3, Evans et al., 2012 and references therein), the higher magnitude (between 3.2 and 4.2) of the earthquakes in Los

253   Potreros suggests that they may be more likely of volcano-tectonic origin due to shallow magma emplacement.

254   In order to further support the above inferences derived from interpretation of the field observations, analogue models

255   were used to constrain the magma source depth from the geometrical parameters measured in the experiments (L_g, θ, α,

256   Table 3).

257   Since our results confirm that the graben width shows a linear correlation with the source depth (fig. 7) as estimated in

258   (Brothelande and Merle, 2015), we calculated the theoretical overburden thickness (i.e. the intrusion depth, T_t, Table 3)

259   as follows:

260    $$T_t = \frac{1}{2}L_g \times \frac{\sin(\theta+\alpha)}{\cos\theta}$$ (1)

261   Comparing the percentage difference between the imposed experimental (T) and theoretical (T_t) overburden thickness

262   values, we calculate the associated error in the evaluation of the intrusion depth in the models (σ, Table 3, Fig.7). We then

263   use equation 1 for the evaluation of the heat source depth at the Loma Blanca bulge considering σ ~ 40 % (maximum

264   value of the experiments).

265   Considering that for the Loma Blanca bulge L_g= 286 m, θ= 71°, α= 4.5°, it follows that the estimated intrusion depth is

266   425 ± 170 m. Such relatively shallow depth is within the range of depths of rhyolitic-dacitic domes drilled in geothermal

267   wells (spanning from 300 to 1700 m, Fig. 1b-c) and is consistent with the hypothesis that the uplift is driven by small and

268   delocalized magmatic intrusions, as suggested by the field data.

269   Even if such rhyolites-dacites have been previously interpreted of subaerial origin (Carrasco-Núñez et al., 2017a), we

270   suggest that such lavas can be reinterpreted as intrusion of felsic cryptodomes based on the following considerations: i)

271   the occurrence of rhyolite-dacite lava bodies within the thick pre-caldera old andesite sequence is unusual and does not

272   have a subaerial counterpart; ii) the intracaldera ignimbrite sequence does not level out the paleotopography; in facts the

273   "topographic high" formed by the rhyolite body in well H-20 (Fig. 1c) persists during the post-caldera emplacement

274   controlling the reduced thickness of lavas of the post caldera stage at that locality; iii) The high depth variation of the top

275   of the Xaltipan ignimbrite not associated with an equal variation of the pre caldera andesite (Fig. 1b) highlighting a local

276   and discontinuous deformation and uplifting of the Xaltipan ignimbrite. These evidences can be more easily reconciled

277   with the intrusion of felsic cryptodomes within the volcanic sequence, respect to a regular layer cake stratigraphy.

278   Summarizing, the combination of field and modelling data support that the uplift in Los Potreros is due to multiple

279   deformation sources in narrow areas that do not represent a resurgence sensu stricto. Such delocalized recent deformation

280   within Los Potreros caldera appears to be linked to small magmatic intrusions located at relatively shallow depths (i.e. <

281   1 km) as in Loma Blanca, where the estimated intrusion depth calculated from the experimental data is 425 ± 170 m.

282   Such model is slightly different from the general accepted idea of resurgence in Los Potreros induced by the inflation of

283   a saucer or cup shaped deep magmatic intrusion (Norini et al., 2015). The resurgence is inferred to be centred beneath the

284   sector of the caldera traversed by the E-W lineaments and delimited by the Maztaloya and Arroyo Grande faults (sector

285   S1 in Norini et al., 2015). The thermal anomalies identified by (Norini et al., 2015) show that the temperatures are

286   unexpectedly cold beneath the inferred centre of the resurgent block, where the highest temperatures should instead be

287   expected. By contrast, sharp and narrow temperature peaks, spatially coincident with Los Humeros and Loma Blanca

288   faults, are consistent with the presence of shallow and delocalized heat sources. Indeed, the inflation of the deep magma

289   chamber of the LHVC, inferred to be at 5 to 7-8 km of depth (Verma, 1983, 2000, 2011) and extending 9 km in radius

290   and 6 km in length (thus coinciding with the Los Humeros caldera rim, Verma et al., 1990), should have resulted in a

291   much wider uplift and with higher magnitude than the one observed in the field. Indeed, resurgence resulting from magma

292   remobilization of the deep chamber that produced the collapse is characterized by a larger-scale surface deformation

293   (thousands of meters of uplift extending for tens of kilometers on the surface) as shown in many large calderas worldwide

294   (Toba, de Silva et al., 2015; Cerro Galan, Folkes et al., 2011; Ischia, Carlino, 2012).

295   It is therefore unlikely that the replenishment of new magma in the caldera forming deep magma chamber accounts for

296   the magnitude (few tens of meters) and discontinuous spatial distribution of the deformation in Los Potreros.

297   Such model of the recent uplifting in Los Potreros is also supported by field-based petrographic-mineralogical analysis

298   showing that the present-day magmatic plumbing system is characterized by multiple magma levels spanning from a deep

299   (30-33 km) basaltic reservoir to very shallow (~ 1.5 km) trachyandesitic-trachytic smaller magma batches (Lucci et al.,

300   under review).

301   A similar model of the plumbing system has been also proposed to explain the historical eruptive activity (since 1663) of

302   Usu volcano (Japan), a post caldera cone of the Toya caldera consisting of a basaltic main edifice surmounted by 3 felsic

303   lava domes and more than 10 cryptodomes. Indeed, petrochemical data suggest the presence of multiple magma batches

304   (i.e. sills) in a depth range of 0.25-2 km that originated from partial melting at various degrees of a metagabbro

305   (Matsumoto and Nakagawa, 2010; Tomya et al., 2010).

306 Our proposed model has crucial implications for planning the future geothermal exploration: future geothermal wells
307 should consider that the local geothermal gradient may be affected by the presence of shallow heat sources within the
308 caldera complicating the pattern of isotherms associated with the deeper heat flow.

309 **6 Conclusions**

310 This study, integrating field work with analogue models, allowed to reconstruct the spatio-temporal evolution of the recent
311 the formation in Los Potreros and estimate the depth of intrusions representing the local heat sources for geothermal
312 exploitation. Our results suggest the following:
313 1. The distribution of the alteration patterns and deformation of the Cuicuiltic member suggests that the recent (post-
314 caldera collapse) uplift in Los Potreros moved from the south and north-eastern sector of the caldera towards N along the
315 Los Humeros and Loma Blanca scarps.
316 2. The estimated depth of the intrusions responsible for such uplift is very shallow, as calculated from the experimental
317 data for the Loma Blanca bulge (425 ± 170 m).
318 3. The recent uplift in Los Potreros is discontinuous in space and time, inducing small-scale (< 1 km) deformations
319 originating from multiple and shallow (< 1 km) magmatic bodies thus not representing a classic resurgent caldera i.e. a
320 large scale (several km) deformation of a single area.

321 **Acknowledgements**

322 CFE is kindly acknowledged for allowing work on the Los Humeros geothermal field. Federico Galetto helped for laser
323 scanner data processing. Fabio Corbi and Matteo Trolese provided technical support in building the experimental set-up.
324 Gianluca Norini is acknowledged for logistic support in the field. Alessandra Pensa kindly helped with figure drawings.
325 Funded by the European Union's Horizon 2020 GEMex Project (grant agreement No. 727550) and by the Mexican Energy
326 Sustainability Fund CONACYT-SENER, WP 4.5 of the Project 2015-04-268074. More information can be found on the
327 GEMex Website: http://www.gemex-h2020.eu. The Grant to Department of Science, Roma Tre University (MIUR-Italy
328 Dipartimenti di Eccellenza, ARTICOLO 1, COMMI 314 – 337 LEGGE 232/2016) is gratefully acknowledged.

329 **References**

330 Acocella, V., Cifelli, F., and Funiciello, R.: The control of overburden thickness on resurgent domes, J. Volcanol. Geoth.
331 Res., 111, 137–153, https://doi.org/10.1016/S0377-0273(01)00224-4, 2001.
332 Arellano, V.M., García, A., Barragán, R.M., Izquierdo, G., Aragón, A., and Nieva, D.: An updated conceptual model of
333 the Los Humeros geothermal reservoir (Mexico), J. Volcanol. Geoth. Res., 124, 67–88, https://doi.org/10.1016/S0377-
334 0273(03)00045-3, 2003.
335 Brothelande, E., Peltier, A., Got, J.L., Merle, O., Lardy, M., and Garaebiti, E.: Constraints on the source of resurgent
336 doming inferred from analogue and numerical modeling — Implications on the current feeding system of the Yenkahe
337 dome–Yasur volcano complex (Vanuatu), J. Volcanol. Geoth. Res., 322, 225–240,
338 https://doi.org/10.1016/j.jvolgeores.2015.11.023, 2016.
339 Brothelande, E., and Merle, O.: Estimation of magma depth for resurgent domes: An experimental approach, Earth Planet.
340 Sc. Lett., 412, 143–151, https://doi.org/10.1016/j.epsl.2014.12.011, 2015.
341 Calcagno, P., Evanno, G., Trumpy, E., Carlos Gutiérrez-Negrín, L., MacIás, J.L., Carrasco-Núñez, G., and Liotta, D.:
342 Preliminary 3-D geological models of Los Humeros and Acoculco geothermal fields (Mexico)-H2020 GEMex Project,
343 Adv. Geosci., 45, 321–333, https://doi.org/10.5194/adgeo-45-321-2018, 2018.
344 Carlino, S.: The process of resurgence for Ischia Island (southern Italy) since 55 ka: The laccolith model and implications
345 for eruption forecasting, B. Volcanol., 74, 947–961. https://doi.org/10.1007/s00445-012-0578-0, 2012.

346 Carrasco-Núñez, G., and Branney, M.J.: Progressive assembly of a massive layer of ignimbrite with a normal-to-reverse
347 compositional zoning: The Zaragoza ignimbrite of central Mexico, B. Volcanol., 68, 3–20,
348 https://doi.org/10.1007/s00445-005-0416-8, 2005.

349 Carrasco-Núñez, G., McCurry, M., Branney, M.J., Norry, M., and Willcox, C.: Complex magma mixing, mingling, and
350 withdrawal associated with an intra-Plinian ignimbrite eruption at a large silicic caldera volcano: Los Humeros of central
351 Mexico, Bull. Geol. Soc. Am., 124, 1793–1809, https://doi.org/10.1130/B30501.1, 2012.

352 Carrasco-Núñez, G., López-Martínez, M., Hernández, J., and Vargas, V.: Subsurface stratigraphy and its correlation with
353 the surficial geology at Los Humeros geothermal field, eastern Trans-Mexican Volcanic Belt, Geothermics, 67, 1–17,
354 https://doi.org/10.1016/j.geothermics.2017.01.001, 2017a.

355 Carrasco-Núñez, G., Hernández, J., De León, L., Dávila, P., Norini, G., Bernal, J.P., Jicha, B., Navarro, M., López-Quiroz,
356 P., and Digitalis, T.: Geologic Map of Los Humeros volcanic complex and geothermal field, eastern Trans-Mexican
357 Volcanic Belt, Terra Digitalis, 1, 1–11, https://doi.org/10.22201/igg.terradigitalis.2017.2.24.78, 2017b.

358 Carrasco-Núñez. G., Bernal, J.P., Dávila, P., Jicha, B., Giordano, G., and Hernández, J.: Reappraisal of Los Humeros
359 volcanic complex by new U/Th zircon and 40Ar/39Ar dating: Implications for greater geothermal potential, Geochem.
360 Geophy. Geosy., 19, 132-149, https://doi.org/10.1002/2017GC007044, 2018.

361 Dávila-Harris, P., and Carrasco-Núñez, G.: An unusual syn-eruptive bimodal eruption: The Holocene Cuicuiltic Member
362 at Los Humeros caldera, Mexico, J. Volcanol. Geoth. Res., 271, 24–42, https://doi.org/10.1016/j.jvolgeores.2013.11.020,
363 2014.

364 de Silva, S.L., Mucek, A.E., Gregg, P.M., and Pratomo, I.: Resurgent Toba - field, chronologic, and model constraints on
365 time scales and mechanisms of resurgence at large calderas, Front. Earth Sci., 3, 1–17,
366 https://doi.org/10.3389/feart.2015.00025, 2015.

367 Doblas, M.: Slickenside kinematic indicators, Tectonophysics, 295, 187–197, https://doi.org/10.1016/S0040-
368 1951(98)00120-6, 1998.

369 Evans, K.F., Zappone, A., Kraft, T., Deichmann, N., and Moia, F.: A survey of the induced seismic responses to fluid
370 injection in geothermal and CO_2 reservoirs in Europe, Geothermics, 41, 30-54,
371 https://doi.org/10.1016/j.geothermics.2011.08.002, 2012.

372 Ferrari, L., Orozco-Esquivel, T., Manea, V., and Manea, M.: The dynamic history of the Trans-Mexican Volcanic Belt and
373 the Mexico subduction zone, Tectonophysics, 522–523, 122–149, https://doi.org/10.1016/j.tecto.2011.09.018, 2012.

374 Ferriz, H., and Mahood, G.A.: Eruption Rates and Compositional Trends at Los Humeros Volcanic Center, Puebla,
375 Mexico, J. Geophys. Res., 89, 8511-8524, https://doi.org/10.1029/JB089iB10p08511, 1984.

376 Folkes, C.B., Wright, H.M., R.A.F. Cas, de Silva, S.L., Lesti, C., and Viramonte, J.G.: A re-appraisal of the stratigraphy
377 and volcanology of the Cerro Galán volcanic system, NW Argentina, B. Volcanol., 73, 1427–1454,
378 https://doi.org/10.1007/s00445-011-0459-y, 2011.

379 Galetto, F., Acocella, V., and Caricchi, L.: Caldera resurgence driven by magma viscosity contrasts, Nat. Commun., 8, 1–
380 11, https://doi.org/10.1038/s41467-017-01632-y, 2017.

381 Guillou-Frottier, L., Burov, E.B., and Milési, J.P.: Genetic links between ash-flow calderas and associated ore deposits as
382 revealed by large-scale thermo-mechanical modelling, J. Volcanol. Geoth. Res., 102, 339–361,
383 https://doi.org/10.1016/S0377-0273(00)00246-8, 2000.

384 Kennedy, B., Wilcock, J., and Stix, J.: Caldera resurgence during magma replenishment and rejuvenation at Valles and
385 Lake City calderas, B. Volcanol., 74, 1833–1847, https://doi.org/10.1007/s00445-012-0641-x, 2012.

386 Kennedy, B., Stix, J., Hon, K., Deering, C., and Gelman, S.: Magma storage, differentiation, and interaction at Lake City
387 caldera, Colorado, USA, Bull. Geol. Soc. Am., 128, 764–776, https://doi.org/10.1130/b31305.1, 2016.

388 Lindsay, J., Emmermann, R., Wemmer, K., de Silva, S., and Trumbull, R.: La Pacana caldera, N. Chile: a re-evaluation
389 of the stratigraphy and volcanology of one of the world's largest resurgent calderas, J. Volcanol. Geoth. Res., 106, 145–
390 173, https://doi.org/10.1016/s0377-0273(00)00270-5, 2001.

391 Lipman, P.W., Zimmerer, M.J., and McIntosh, W.C.: An ignimbrite caldera from the bottom up: Exhumed floor and fill
392 of the resurgent Bonanza caldera, Southern Rocky Mountain volcanic field, Colorado, Geosphere, 11, 1902–1947,
393 https://doi.org/10.1130/GES01184.1, 2015.

394 Lermo, J., Lorenzo, C., Jiménez, N., Ramos, E., Ângulo, J., Israel, J., Téllez, N., Machado, O., Álvarez, I., Torres, R.,
395 Alfaro R.: Analisis de la actividad sismica (1994-2016), su relacion con los pozos inyectores y productores y aplicación
396 de nuevas tecnicas geofisica para caracterizar las zonas anómalas del campo geotérmico de Los Humeros, CEMIE-GEO,
397 Mexico, Internal Rep., 42 pp., 2018.

398 Lucci, F., Carrasco-Núñez, G., Rossetti, F., Theye, T., White, J. C., Urbani, S., Azizi, H., Asahara, Y., and Giordano, G.:
399 Anatomy of the magmatic plumbing system of Los Humeros Caldera (Mexico): implications for geothermal systems,
400 Solid Earth Discuss., https://doi.org/10.5194/se-2019-86, in review, 2019.

401 Marsh, B.D.: On the mechanics of caldera resurgence, J. Geophys. Res., 89, 8245–8251,
402 https://doi.org/10.1029/JB089iB10p08245, 1984.

403 Merle, O., Borgia, A.: Scaled experiments of volcanic spreading, J. Geophys. Res., 101, 13805-13817,
404 https://doi.org/10.1029/95JB03736, 1996.

405 Métrich, N., Allard, P., Aiuppa, A., Bani, P., Bertagnini, A., Shinohara, H., Parello, F., Di Muro, A., Garaebiti, E., Belhadj,
406 O., and Massare, D.: Magma and volatile supply to post-collapse volcanism and block resurgence in Siwi caldera (Tanna
407 Island, Vanuatu arc), J. Petrol., 52, 1077–1105, https://doi.org/10.1093/petrology/egr019, 2011.

408 Mueller, W.U., Stix, J., Corcoran, P.L., Daigneault, R.: Subaqueous calderas in the Archean Abitibi greenstone belt: An
409 overview and new ideas, Ore Geol. Rev., 35, 4–46, https://doi.org/10.1016/j.oregeorev.2008.12.003, 2009.

410 Norini, G., Groppelli, G., Sulpizio, R., Carrasco-Núñez, G., Dávila-Harris, P., Pellicioli, C., Zucca, F., and De Franco, R.:
411 Structural analysis and thermal remote sensing of the Los Humeros Volcanic Complex: Implications for volcano structure
412 and geothermal exploration, J. Volcanol. Geoth. Res., 301, 221–237, https://doi.org/10.1016/j.jvolgeores.2015.05.014,
413 2015.

414 Matsumoto, A., and Nakagawa, M.: Formation and evolution of silicic magma plumbing system: Petrology of the volcanic
415 rocks of Usu volcano, Hokkaido, Japan, J. Volcanol. Geoth. Res., 196, 185–207,
416 https://doi.org/10.1016/j.jvolgeores.2010.07.014, 2010.

417 Pribnow, D.F.C., Schütze, C., Hurter, S.J., Flechsig, C., Sass, J.H.: Fluid flow in the resurgent dome of Long Valley
418 Caldera: Implications from thermal data and deep electrical sounding. J. Volcanol. Geoth. Res., 127, 329–345,
419 https://doi.org/10.1016/S0377-0273(03)00175-6, 2003.

420 Stix, J., Kennedy, B., Hannington, M., Gibson, H., Fiske, R., Mueller, W., Franklin, J.: Caldera-forming processes and the
421 origin of submarine volcanogenic massive sulfide deposits, Geology, 31, 375–378, https://doi.org/10.1130/0091-
422 7613(2003)031<0375:CFPATO>2.0.CO;2, 2003.

423 Tomiya, A., Takahashi, E., Furukawa, N., Suzuki, T.: Depth and evolution of a silicic magma chamber: Melting
424 experiments on a low-K rhyolite from Usu volcano, Japan, J. Petrol., 51, 1333–1354,
425 https://doi.org/10.1093/petrology/egq021, 2010.

426   Verma, M.P., Verma, S.P., and Sanvicente, H.: Temperature field simulation with stratification model of magma chamber
427   under Los Humeros caldera, Puebla, Mexico, Geothermics, 19, 187–197, https://doi.org/10.1016/0375-6505(90)90015-
428   4, 1990.
429   Verma, S.P., Gómez-Arias, E., and Andaverde, J.: Thermal sensitivity analysis of emplacement of the magma chamber in
430   Los Humeros caldera, Puebla, Mexico, Int. Geol. Rev., 53, 905–925, https://doi.org/10.1080/00206810903234296, 2011.
431   Verma, S.P.: Magma genesis and chamber processes at Los Humeros caldera, Mexico - Nd and Sr isotope data, Nature,
432   302, 52–55, https://doi.org/10.1038/302052a0, 1983.
433   Verma, S.P.: Geochemical evidence for a lithospheric source for magmas from Los Humeros caldera, Puebla, Mexico.
434   Chem. Geol. 164, 35–60, https://doi.org/10.1016/S0009-2541(99)00138-2, 2000.
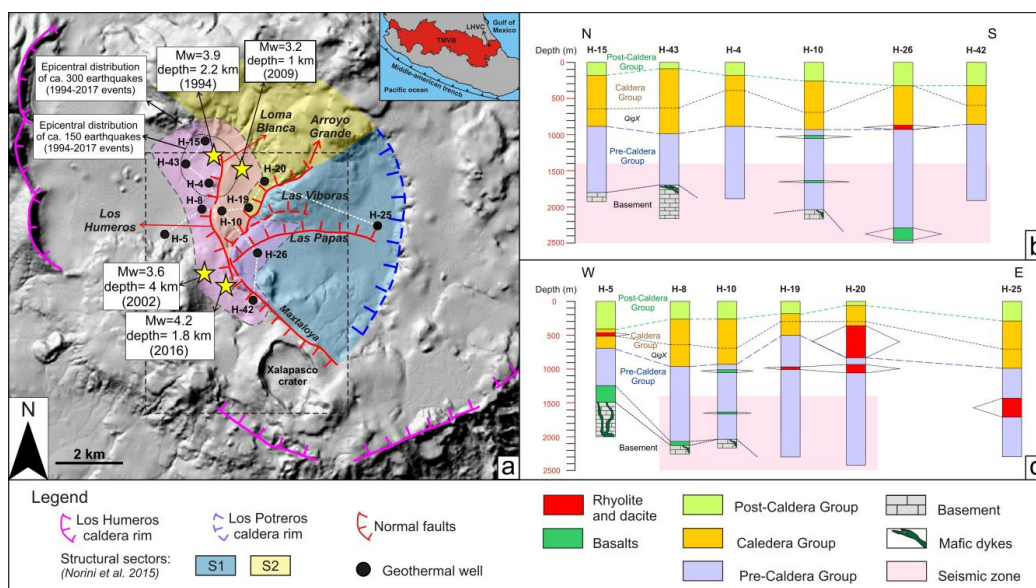
Figure 1: a) Shaded relief image (illuminated from the NE) obtained from 15 m resolution DEM of the Los Humeros Volcanic Complex (LHVC) showing the main structural features (faults and caldera rim, modified from Norini et al., 2015; Calcagno et al., 2018) and some geothermal wells referred in the text. In depth correlation of lithostratigraphic units along the N-S (b) and W-E (c) direction (redrawn after Carrasco-Núñez et al., 2017a and Arellano et al., 2003)., Depth:horizontal distance=1:1. Location of the correlation line is shown in a). QigX= Xaltipan ignimbrite. The black rectangle indicates the studied area within the Los Potreros Caldera shown in figure 3. The Inset box show the location of the LHVC (black dot and arrow) within the eastern sector of the Trans Mexican Volcanic Belt (TMVB). The structural sectors S1 and S2 correspond to the resurgent block inferred by (Norini et al., 2015). Seismicity data from (Lermo et al., 2018).
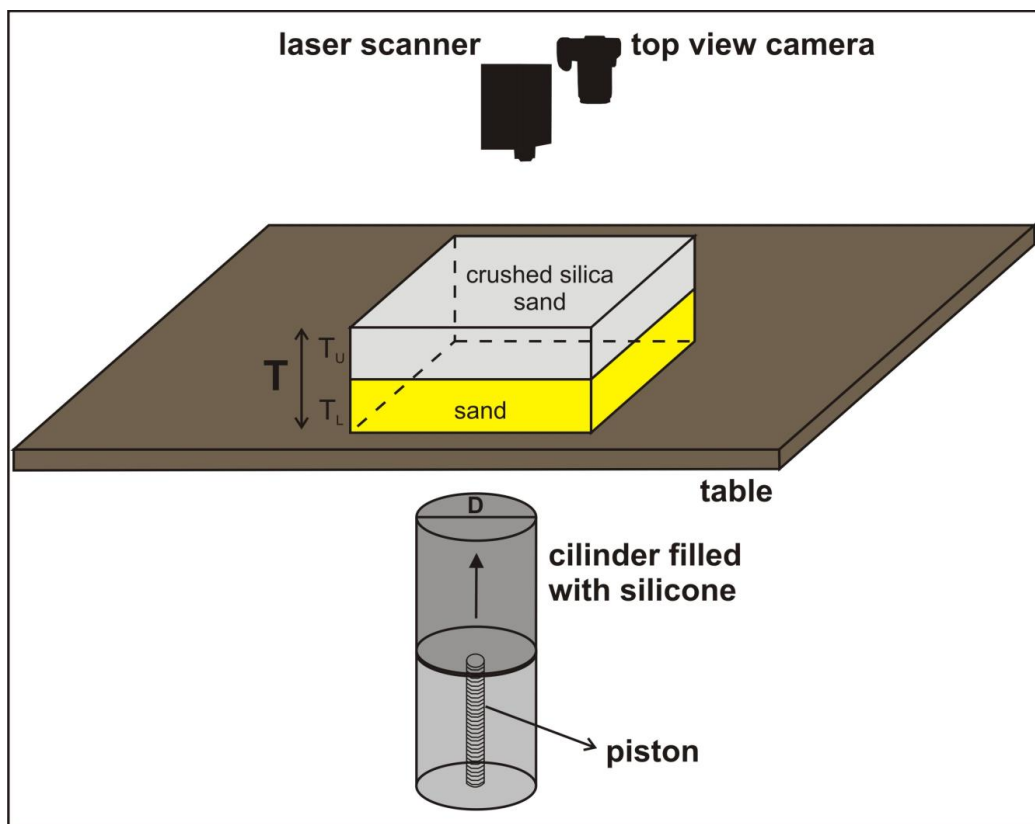
444
445 **Figure 2: Experimental set-up. D= diameter of the cylinder.**
446
447
448
449
450
451
452
453
454
455
456
457
458
459
460
461
462
463
464
465
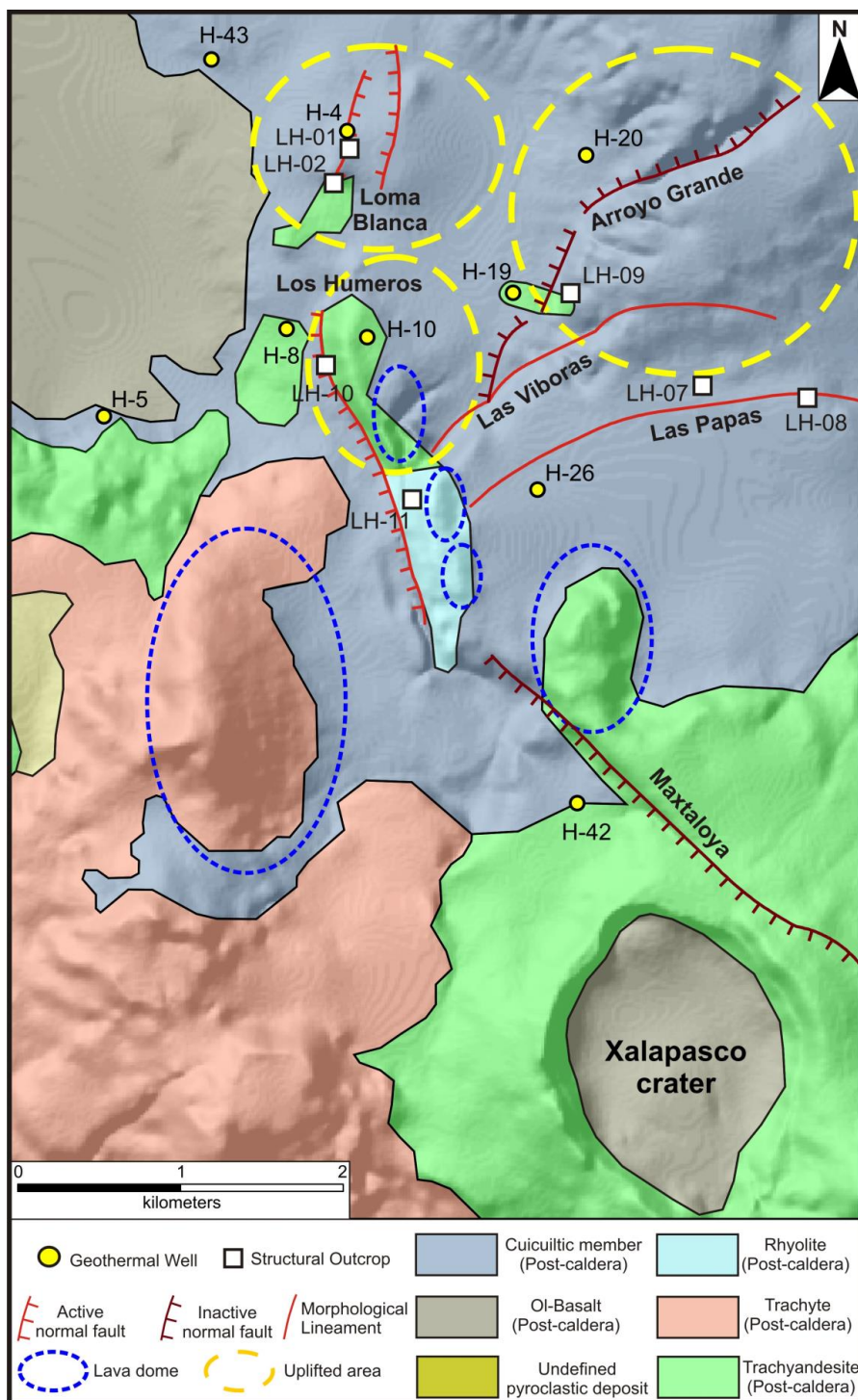
Figure 3: Simplified geological structural map of the studied area reinterpreted after (Norini et al., 2015; Carrasco- Núñez et al., 2017b; Calcagno et al., 2018).
Figure 4: a) Panoramic view from Xalapasco crater (looking towards N) of the rhyolitic lava domes aligned N-S. **b)** Panoramic view of the E-W trending Las Papas scarp. **c)** Unaltered Cuicuiltic (LH-07). **d)** Unaltered Cuicuiltic covering a layered pyroclastic deposit (LH-08). The erosional surface preceding the deposition of the Cuicuiltic is shown (dashed white line).
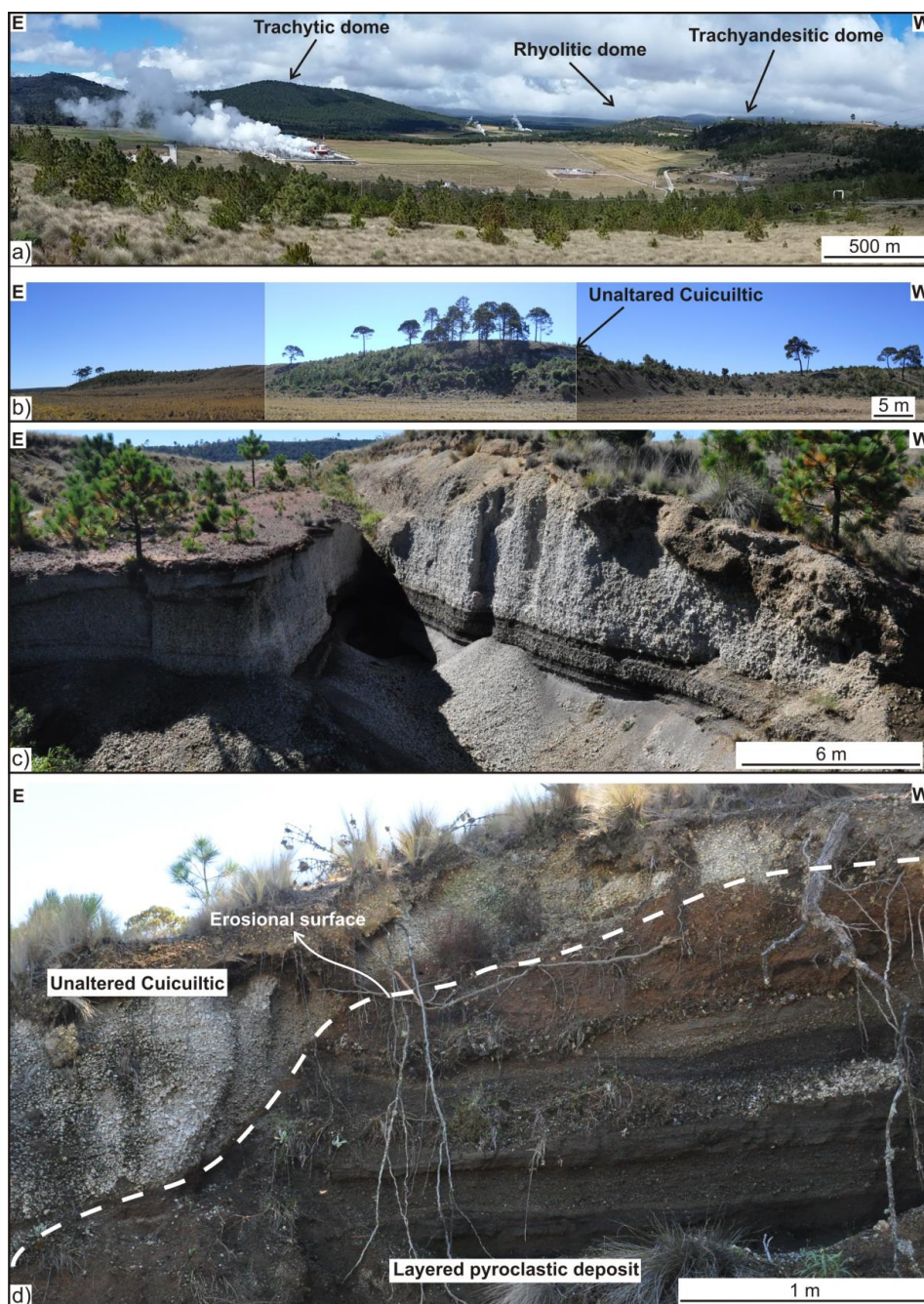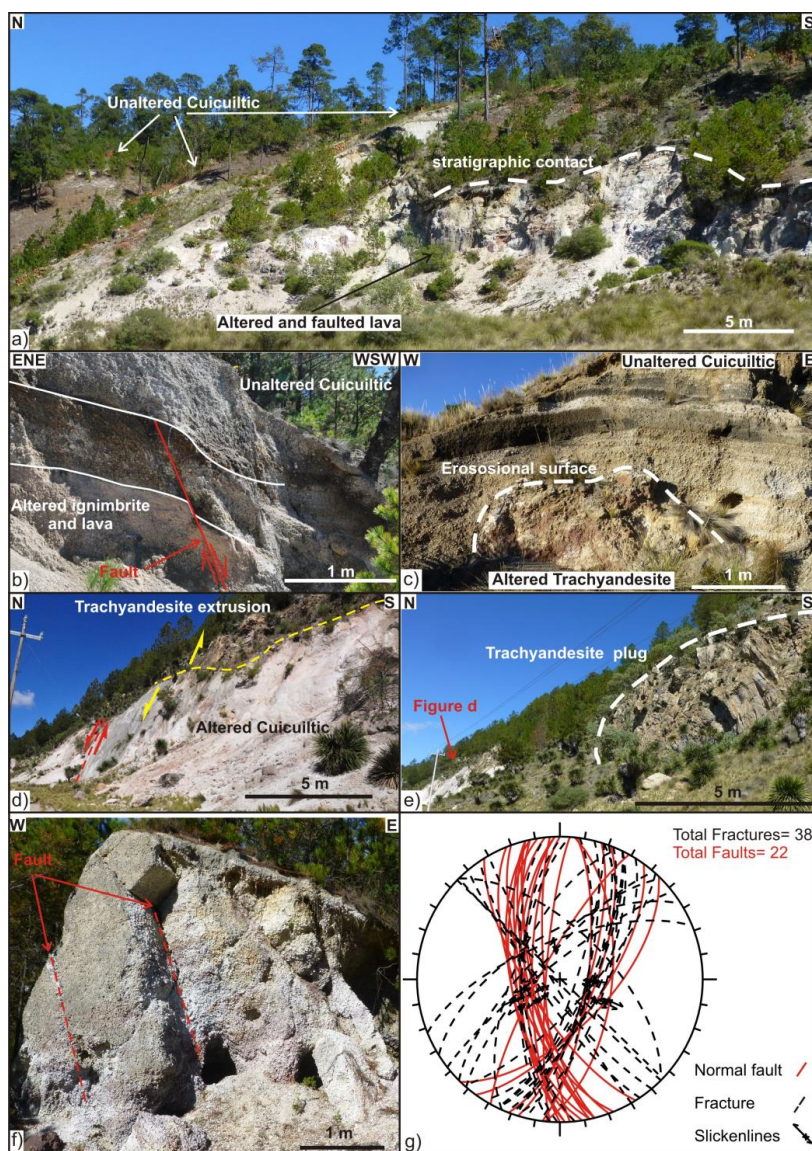
473
474 **Figure 5: a) Panoramic view of the Arroyo Grande fault scarp showing the Unaltered Cuicuiltic covering the altered and faulted**
475 **ignimbrite and lavas. b) Normal fault affecting the altered ignimbrite deposits unconformably covered by the post-caldera,**
476 **unaltered Cuicuiltic deposits (LH-09). Note that the Cuicuiltic deposits are not faulted at this location; the fault can be thus**
477 **considered as a fossil fault with respect to the Cuicuiltic deposition. c) Block of altered trachyandesite buried by unaltered**
478 **Cuicuiltic layers along the Maztaloya fault scarp. d) Los Humeros fault scarp (LH-10) induced by the ascent of the rhyolitic**
479 **extrusion on top of the fault plane. e) Rhyolitic plug cropping out ~150 southward the fault scarp shown in d) (indicated by the**
480 **red arrow). f) Normal faulting and alteration of the Cuicuiltic member within the apical graben of the Loma Blanca dome (site**
481 **LH-01). e) Equal-area stereo-plot of the attitudes of faults and fractures in all the structural outcrops.**
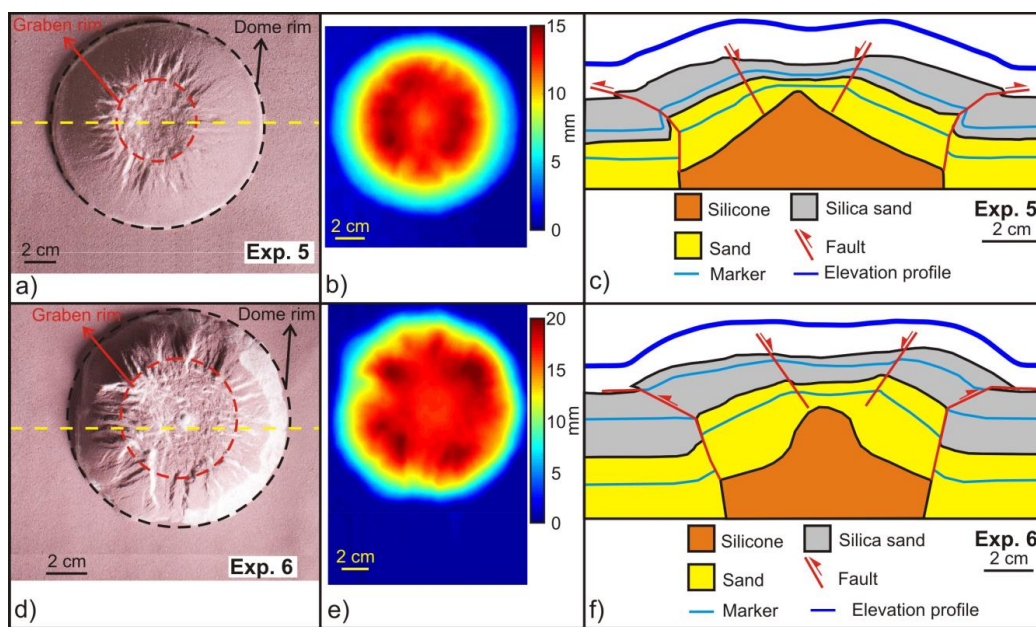
Figure 6: a) d) Top view image of the experiments 5 and 6. b) e) cumulative vertical displacement; colour scale is proportional to the amount of uplift. c) f) Drawing of the cross section view obtained after cutting the section close to the dome center. The elevation profiles are obtained from laser scanner data. The yellow dashed line in the top view images indicates the trace of the section views and of the elevation profiles.

482
483
484
485
486
487
488
489
490
491
492
493
494
495
496
497
498
499
500
501
502
503
504
505
506
507
508
509
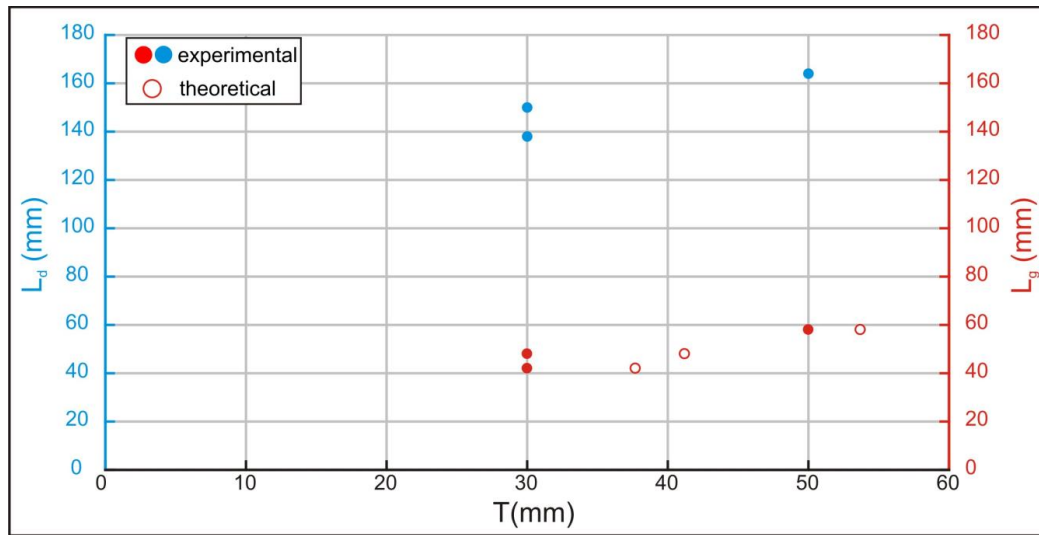
Figure 7: L_g (graben width) and L_d (dome diameter) versus T. Theoretical values calculated after equation 1 (see discussion section).

$$L_g \text{ (graben width) and } L_d \text{ (dome diameter) versus T.}$$
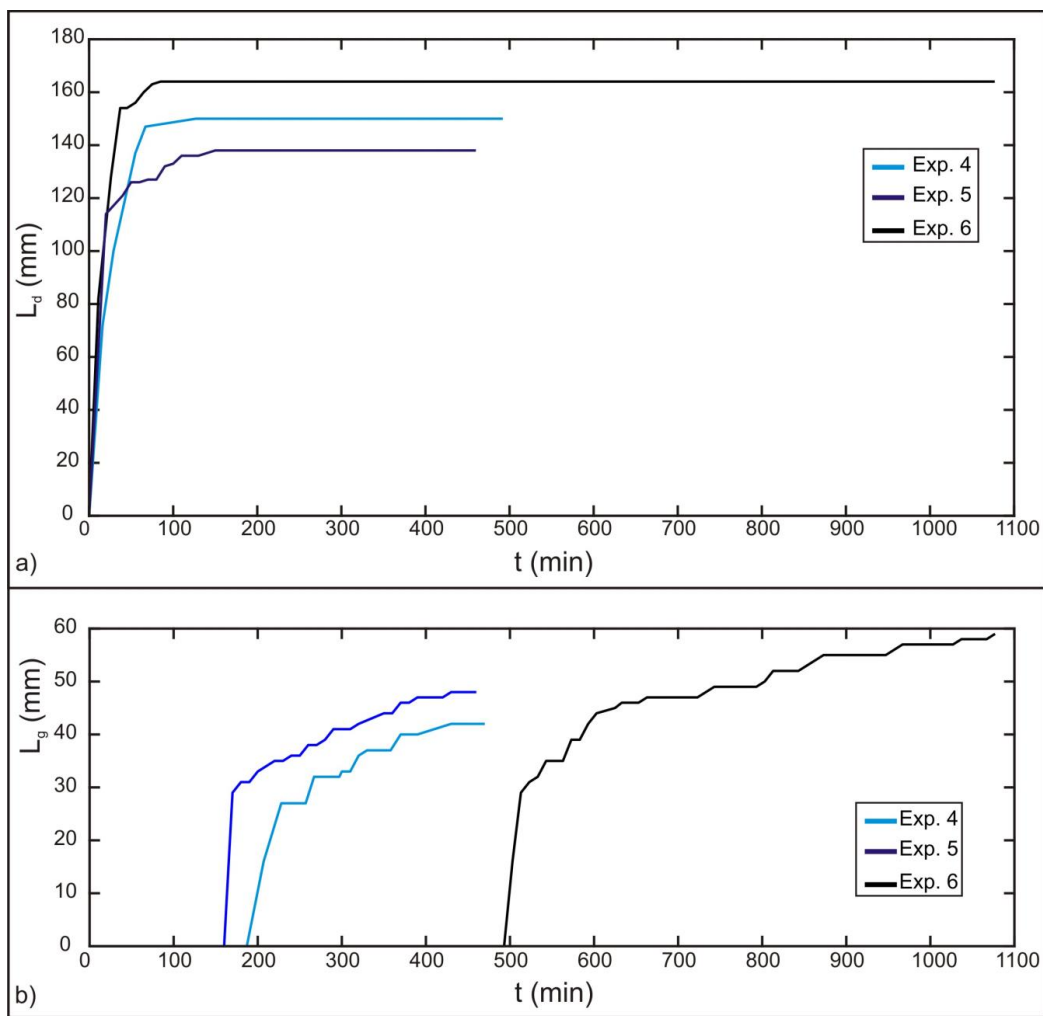
513
514   **Figure 8: a) L$_d$ versus time b) L$_g$ versus time.**
515
516
517
518
519
520
521
522
523
524
525
526
527
528

529
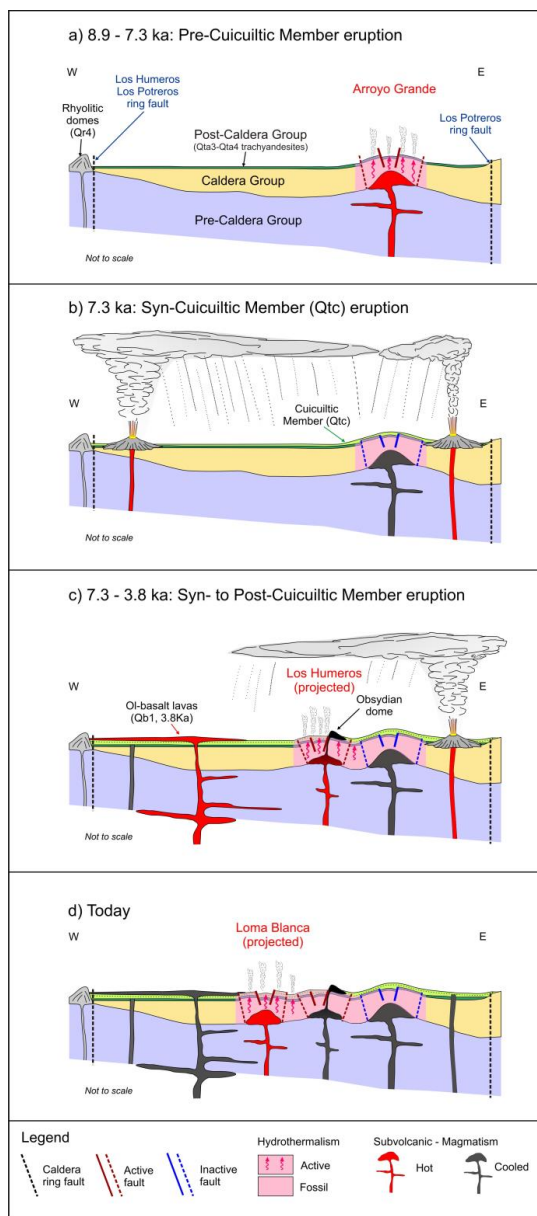
Figure 9: Schematic model of the evolution of the sub-surface structure of the Los Potreros caldera floor. Multiple magmatic intrusions located at relatively shallow depth (< 1 km) are responsible for the localized bulging of the caldera floor (Loma Blanca, Los Humeros and Arroyo Grande uplifted areas). a) Pre Cuicuiltic stage: emplacement of a felsic intrusion at shallow depth and formation of the Arroyo grande bulge characterized by extensional faulting at its top, reverse faulting at its base and hydrotermalism. b) Syn-Cuicuiltic stage: eruption of the Cuicuiltic member covering the hydrothermally altered post-caldera trachyandesitic lavas. c) Syn to post Cuicuiltic stage: formation of the Los Humeros fault and extrusion of obsidian lava domes along the fault scarp. As the trachyandesitic domes are covered with Cuicuiltic member only at his base, the lava extrusion occurred during and post the Cuicuiltic eruption. d) Formation of the Loma Blanca bulge with the current hydrothermal activity and extensional faulting occurring within the apical graben.

Parameter	Definition	Value
T	Thickness of the sand overburden	$1\text{-}5 \times 10^{-2}$ m
L_d	dome diameter	$1\text{-}1.6 \times 10^{-1}$ m
H	Dome height	$1.3\text{-}2 \times 10^{-2}$ m
ρ_s	sand density	1400 kg/m^3
ϕ	Angle of internal friction of sand	25-40°
τ_0	Sand cohesion	300 Pa
ρ_m	silicone density	1000 kg/m^3
μ_m	silicone viscosity	10^4 Pa s
g	Gravity	9.8 m/s^2
t	Experiment duration	$2\text{-}6.5 \times 10^4$ s

539   **Table 1. Geometric and material properties parameters of the experiments.**

Dimensionless ratio	Experiments	Nature
$\Pi_1 = T/L_d$	0.1-0.6	0.04–0.6
$\Pi_2 = H/L_d$	0-0.12	0-0.12
$\Pi_3 = \rho_s/\rho_m$	1.4	0.6-1.4
$\Pi_4 = \phi$	35	25-40
$\Pi_5 = \rho_m H^2/\mu_m t$	6×10^{-10}	1.8×10^{-8}
$\Pi_6 = \rho_m g H t/\mu_m$	1.3×10^3	6.9×10^2
$\Pi_7 = \rho_s g T/\tau_0$	4.57	8.24

540   **Table 2. Definition and values of the dimensionless ratios Π in nature and in the experiments.**

Exp	T (mm)	L_g (mm)	L_d (mm)	θ	α	T_t (mm)	σ (%)
4	30	42	150	58°	14°	37.7	27
5	30	48	138	56°	18°	41.2	37
6	50	58	164	58°	21°	53.7	7

541   **Table 3. Measured parameters in the experiments. T=overburden thickness; L_d= dome diameter; L_g=graben width; θ= graben**

542   **fault dip; α= dome flank mean dip; T_t= theoretical overburden thickness calculated with equation 1 (Brothelande and Merle,**

543   **2015, see discussion section); σ= percentage difference between T and T_t.**